JOURNAL OF GUIDANCE, CONTROL, AND DYNAMICS
Vol. 29, No. 1, January–February 2006

Nonlinear Recursive Estimation of Boost Trajectories, Including Batch Initialization and Burnout Estimation

Michael E. Hough*
Raytheon Company, Woburn, Massachusetts 01801

A 12-state, iterated nonlinear recursive filter is formulated for boost trajectory estimation and prediction. The recursive filter is initialized with state and covariance estimates from a polynomial batch filter. An interacting multiple-model technique handles staging and burnout events by statistically blending boost filter estimates with estimates from a Keplerian filter. A new contribution is a boost prediction model that includes terms that model the nonlinear growth of thrust acceleration magnitude caused by propellant consumption and variations in thrust orientation associated with gravity-turn maneuvers and steering maneuvers at constant or variable angles of attack. State estimates and covariances are iterated at each filter update, subject to constraints on magnitude and orientation of the thrust acceleration estimates. These constraints are useful in controlling unrealistic estimates caused by poor measurements, in precluding unbounded acceleration predictions during long intervals without measurements, and in handling acceleration discontinuities at staging events. A noteworthy feature is that this algorithm does not rely on any a priori information such as a booster template.

I. Introduction

MANY different algorithms have been developed for boost trajectory estimation.[1–11] Algorithm selection depends primarily on the information content in the boost sensor measurements. With angle-only measurements from one sensor, batch filters are preferred and an a priori trajectory profile (or template) supplements the incomplete position information in the two-dimensional measurements.[3,6,7] Nonlinear recursive filters can be used with three-dimensional position measurements, and the template may be replaced with nonlinear prediction models.[1,2,4,5,8–11] These physics-based models allow real-time adaptation to the measurement data and improve accuracies of sensor cues and predicted aimpoints for boost phase intercept. Boost trajectory adaptation is important because sudden unpredictable changes in thrust acceleration can occur at missile staging events and at burnout.

An extended Kalman filter (EKF) is the simplest technique for nonlinear estimation of a boost trajectory, and the most elaborate techniques solve the Fokker–Planck equation for the probability distribution (see Ref. 4). In earlier publications, an EKF was formulated with nine state variables for estimation of the inertial components of position, velocity, and thrust acceleration.[5,10] The EKF(9) prediction model includes a vector-differential equation that models 1) the nonlinear changes in thrust acceleration magnitude caused by propellant consumption and 2) thrust-orientation dynamics associated with gravity-turn maneuvers and other booster steering maneuvers at constant angle of attack. In addition to boost trajectories, EKF(9) has been applied to launch point estimation[11] and can be applied to postboost vehicle trajectory estimation.

This paper describes several improvements that enhance the performance of EKF(9). The improvements include the addition of three angular velocity variables, batch filter initialization, iteration of the update with vector constraints on thrust acceleration, and a multiple-model algorithm for staging and burnout events, as follows. A functional diagram of EKF(12) illustrates the interactions of all of these features (Fig. 1).

Steering maneuvers with variable angles of attack generate angular velocities that are not modeled in the EKF(9) prediction model. For EKF(12), a first-order vector-Markov process describes the dynamics of these new angular velocity states.

Initial estimates of the state vector and covariance matrix are generated from position measurements. Classical methods of initial orbit determination, such as Laplace's method for Keplerian orbits (see Ref. 12), are not applicable because thrust acceleration is nonzero. Rather, EKF(12) is initialized by a polynomial batch filter with an approximate (constant jerk) prediction model.

EKF(12) estimates and covariances are iterated at each filter update to mitigate filter nonlinearities and to improve agreement of the filter covariance and the statistics of the actual errors in the estimates. When filter states are sufficiently observable, iteration of the estimates has been shown to approximate a maximum-likelihood estimate using a Gauss–Newton iteration technique (see Refs. 13 and 14).

Boost phase estimates and predictions are constrained by limits on the magnitude and direction of the thrust acceleration. Because poor measurements can cause wild acceleration estimates, these constraints allow the filter to recover on subsequent updates when better information becomes available. Constraints also preclude unbounded thrust accelerations during long prediction intervals without observations, for example, for boost phase intercept applications.

Precise position (and optionally velocity) measurements allow detection of sudden changes in acceleration at staging events and at burnout. An interacting multiple-model (IMM) technique[15–19] blends the estimates and covariances of EKF(12) with those of a six-state Keplerian model EKF(6) (see Ref. 20). Statistical weights are determined using the EKF(12) and EKF(6) measurement residuals and their covariances.

This paper is organized as follows. Boost and Keplerian prediction models are formulated (Sec. II and Appendix A). Nonlinear measurement models are given for angle-only and range-angle sensors (Sec. III). Initialization of EKF(12) with a polynomial batch filter is described (Sec. IV and Appendix B). Iteration of EKF(12) is performed with constraints on thrust acceleration (Sec. V). Boost and Keplerian estimates and covariances are statistically blended with an IMM technique (Sec. VI). Performance analysis results are presented and discussed (Sec. VII). Finally, the paper is summarized and conclusions are drawn (Sec. VIII).

II. Nonlinear Prediction Models

Boost and Keplerian prediction models are needed for the IMM filter (to be discussed later). During boost, the state vector $\boldsymbol{x}$ includes the Cartesian inertial components of the position vector $\boldsymbol{r}$, inertial velocity vector $\boldsymbol{v}$, thrust acceleration vector $\boldsymbol{a}_c$, and Markov angular

Received 30 August 2004; revision received 15 November 2004; accepted for publication 27 November 2004.

*Senior Principal Systems Engineer, 235 Presidential Way. Senior Member AIAA.

Table 1 Boost dynamics model for EKF(12)

Differential equations	Definition of terms
$\dfrac{\mathrm{d}\boldsymbol{x}}{\mathrm{d}t} = \boldsymbol{f}(\boldsymbol{x}) = \begin{bmatrix} \boldsymbol{v} \\ \boldsymbol{a}_c + \boldsymbol{g}(\boldsymbol{r}) \\ \boldsymbol{b}(\boldsymbol{r}, \boldsymbol{v}, \boldsymbol{a}_c, \boldsymbol{\varpi}) \\ -(1/\tau)\boldsymbol{\varpi} \end{bmatrix}$	$\boldsymbol{b} = \dfrac{a_c}{U}\boldsymbol{a}_c + (\boldsymbol{\omega} + \boldsymbol{\varpi}) \times \boldsymbol{a}_c, \qquad U = I_{\mathrm{sp}} g_0$
	$\boldsymbol{\omega} = \dfrac{1}{u^2}\boldsymbol{u} \times (\boldsymbol{g} + \boldsymbol{a}_c)$
	$\boldsymbol{u} = \boldsymbol{v} - \boldsymbol{\omega}_e \times \boldsymbol{r}, \qquad \boldsymbol{g} = -\dfrac{\mu_e}{r^3}\boldsymbol{r}$
	$F(\boldsymbol{x}) = \dfrac{\partial \boldsymbol{f}}{\partial \boldsymbol{x}^T} = \begin{bmatrix} O_3 & I_3 & O_3 & O_3 \\ \Gamma & O_3 & I_3 & O_3 \\ A & B & C & D \\ O_3 & O_3 & O_3 & -(1/\tau) I_3 \end{bmatrix}$
$\dfrac{\mathrm{d}P}{\mathrm{d}t} = F(\boldsymbol{x})P + PF(\boldsymbol{x})^T + Q$	$A = -\dfrac{1}{u^2}\Omega(\boldsymbol{a}_c)\left[\Omega(\boldsymbol{u})\Gamma(\boldsymbol{r}) + \Omega(\boldsymbol{a}_c + \boldsymbol{g})\left(\Omega(\boldsymbol{\omega}_e) - \dfrac{2}{u^2}\boldsymbol{u}\boldsymbol{u}^T\Omega^T(\boldsymbol{\omega}_e)\right)\right]$
	$B = \dfrac{1}{u^2}\Omega(\boldsymbol{a}_c)\Omega(\boldsymbol{a}_c + \boldsymbol{g})\left(I_3 - \dfrac{2}{u^2}\boldsymbol{u}\boldsymbol{u}^T\right)$
	$C = \dfrac{1}{aU}\left(a^2 I_3 + \boldsymbol{a}_c\boldsymbol{a}_c^T\right) + \Omega(\boldsymbol{\omega} + \boldsymbol{\varpi}) - \dfrac{1}{u^2}\Omega(\boldsymbol{a}_c)\Omega(\boldsymbol{u})$
	$D = -\Omega(\boldsymbol{a}_c)$
	$\Gamma = \dfrac{\partial \boldsymbol{g}}{\partial \boldsymbol{r}^T} = \dfrac{\mu_e}{r^5}\left(3\boldsymbol{r}\boldsymbol{r}^T - r^2 I_3\right)$
	$Q = \mathrm{diag}\{\underset{q_a}{0} \quad \underset{q_a}{0} \quad \underset{q_a}{0} \quad \underset{q_\varpi}{0} \quad \underset{q_\varpi}{0} \quad \underset{q_\varpi}{0}\}$

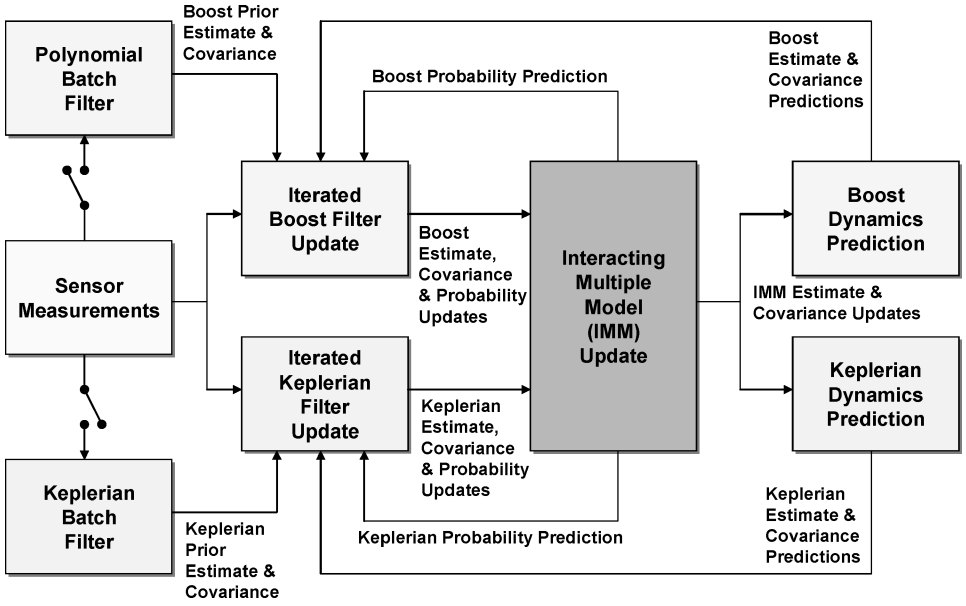

Fig. 1 Functional diagram of estimation algorithm for boost trajectories.

velocity vector $\boldsymbol{\varpi}$:

$$\boldsymbol{x}_n^T = \begin{bmatrix} \boldsymbol{r}^T(t_n) & \boldsymbol{v}^T(t_n) & \boldsymbol{a}_c^T(t_n) & \boldsymbol{\varpi}^T(t_n) \end{bmatrix}$$

For a Keplerian orbit, the number of state variables may be reduced from 12 to 6:

$$\boldsymbol{\xi}_n^T = \begin{bmatrix} \boldsymbol{r}^T(t_n) & \boldsymbol{v}^T(t_n) \end{bmatrix}$$

The EKF(12) prediction model is a system of 90 coupled, nonlinear differential equations (Table 1). The linearized dynamics matrix $F(\boldsymbol{x}) = \partial \boldsymbol{f}/\partial \boldsymbol{x}^T$ couples the 12 differential equations for $\boldsymbol{x}(t)$ with the 78 differential equations for the diagonal and upper triangular elements of the symmetric covariance matrix $P(t)$. Elements of $F(\boldsymbol{x})$ may be determined by partial differentiations of the nonlinear state equations (Appendix A). Errors in $\hat{\boldsymbol{x}}$ cause errors in $F(\hat{\boldsymbol{x}})$ that are not properly compensated in the linear equations for covariance prediction. Consequently, process noise Q is added to improve covariance prediction. A diagonal Q matrix is assigned with constant acceleration variance q_a and constant angular-rate variance q_ϖ. $\Omega(\,)$ is the skew-symmetric cross product matrix:

$$\Omega(\boldsymbol{a}_c) = \begin{bmatrix} 0 & -a_3 & a_2 \\ a_3 & 0 & -a_1 \\ -a_2 & a_1 & 0 \end{bmatrix}, \qquad \Omega(\boldsymbol{\omega}_e) = \begin{bmatrix} 0 & -\omega_e & 0 \\ \omega_e & 0 & 0 \\ 0 & 0 & 0 \end{bmatrix}$$

Nonlinear state equations for EKF(12) model the booster guidance and control process, which is generally unknown. Because booster orientation is stabilized about a rotating Earth-relative velocity $\boldsymbol{u}$, the nonlinear vector-differential equation for $\boldsymbol{a}_c$ includes three angular velocity terms as follows. Early in the ascent, when angle of attack and lateral aerodynamic loads on the booster airframe are minimized, $\boldsymbol{u}$ rotates downward with angular velocity $(\boldsymbol{u} \times \boldsymbol{g})/u^2$, corresponding to a gravity turn. Later in the ascent when the booster

leaves the atmosphere, steering maneuvers cause a misalignment of $\boldsymbol{u}$ and $\boldsymbol{a}_c$, and $\boldsymbol{u}$ rotates with angular velocity $(\boldsymbol{u}\times\boldsymbol{a}_c)/u^2$, corresponding to an accelerated turn at constant angle of attack. Finally, the angular velocity $\boldsymbol{\varpi}$ accounts for rotations of $\boldsymbol{u}$ caused by variable angles of attack and by rotation of the plane defined by $\boldsymbol{u}$ and $\boldsymbol{a}_c$. Because the third class of rotations is weakly correlated to the other state variables, $\boldsymbol{\varpi}$ is described by a first-order vector-Markov process with time constant τ.

Values of the constant parameters τ, q_a, and q_{ϖ} are selected based on a Monte Carlo filter tuning process. (Results are summarized in Table 2.) It will be shown that the recommended values produce filter covariance matrices that are consistent with the simulated error statistics. Satisfactory performance has been demonstrated for many different booster trajectories with the same set of tuning parameters. A typical value of exhaust velocity U is selected to characterize most types of chemical propellants.

In a central, inverse-square gravitational field, EKF(6) state $\boldsymbol{\xi}_n$ and covariance Ξ_n are predicted with nonlinear difference equations corresponding to a Keplerian orbit (see Ref. 20):

$$\boldsymbol{\xi}_{n+1}=\Phi(\boldsymbol{\xi}_n,t_{n+1}-t_n)\boldsymbol{\xi}_n$$

$$\overline{\Xi}_{n+1}=\Phi(\boldsymbol{\xi}_n,t_{n+1}-t_n)\Xi_n\Phi^T(\boldsymbol{\xi}_n,t_{n+1}-t_n)+G_n(\Xi_n)$$

The Keplerian state transition matrix Φ_n may be expressed by a nonlinear function of the state and the elapsed time. In fact, Φ_n actually depends on the central angle (or true anomaly) along the orbit, and Kepler's equation must be solved to relate the change in angle to elapsed time. Process noise G_n is included because errors in $\hat{\boldsymbol{\xi}}_n$ cause errors in Φ_n, and these nonlinear errors are not properly represented in the linearized equations for covariance prediction. Physically, G_n arises from a gravity-gradient disturbance caused by differences between the estimated and true positions. Consequently, $G_n(\Xi_n)$ depends on the covariance matrix, and the tuning process is, therefore, self adaptive. Because the algebraic form of $G_n(\Xi_n)$ is complicated, see Ref. 20 for details.

III. Nonlinear Measurement Model

Three-dimensional position measurements are needed for EKF initialization and tracking. The unit line-of-sight (LOS) vector $\boldsymbol{\lambda}_n$ from sensor to target may be determined from sensor angle measurements of LOS elevation angle γ_n from horizontal and LOS azimuth angle ψ_n from north:

$$\boldsymbol{\lambda}_n=\Re_n^T(\boldsymbol{R}_n)\begin{bmatrix}\sin\gamma_n\\ \cos\gamma_n\sin\psi_n\\ \cos\gamma_n\cos\psi_n\end{bmatrix}$$

where the transformation matrix $\Re_n$ from the inertial frame to the sensor local-level frame depends on the inertial position vector $\boldsymbol{R}_n$ of the sensor. Inasmuch as $\boldsymbol{\lambda}_n$ is a two-dimensional position measurement because $|\boldsymbol{\lambda}_n|=1$, a suite of angle-only sensors is required to triangulate the target. In contrast, one range-angle sensor (such as a radar) measures γ_n, ψ_n, and range distance ρ_n.

The measurement $\boldsymbol{y}_n$ is a nonlinear vector function $\boldsymbol{h}(\boldsymbol{r}_n)$ with components specified in sensor coordinates (Table 3). These well-known identities are repeated for convenience and for later use. Measurement errors $\boldsymbol{\upsilon}_n$ are approximated by additive, zero-mean, uncorrelated Gaussian random variables, and R_n is a diagonal measurement noise matrix. Because $\boldsymbol{y}_n$ and R_n are specified in sensor coordinates (rather than Cartesian-inertial coordinates of the target), the measurement-sensitivity matrix $H(\boldsymbol{x}_n)$ is a nonlinear function. When evaluated for EKF(6), $H(\boldsymbol{\xi}_n)$ has 6 columns rather than 12.

Table 2 EKF(12) parameters

Description	Symbol	Value
Exhaust velocity	U	2450 m/s
Thrust acceleration rms process noise (each axis)	q_a	0.5 m/s$^{5/2}$
Time constant for Markov angular velocity state	τ	100 s
Markov angular velocity rms process noise (each axis)	q_{ϖ}	0.01 deg/s$^{5/2}$

IV. Batch Initialization of the Recursive Filter

Initial estimates of the state vector and covariance matrix are generated from the measurements because prior trajectory information may not be useful. For example, booster detection usually occurs after launch because the launch point is either beyond the visible horizon of ground-based radars or the early ascent is beneath a cloud layer that obscures the infrared plume signature from satellite infrared sensors. Moreover, a vertical-ascent trajectory may be a poor approximation when the booster maneuvers before detection by the sensor.

During the short time interval when observations are collected for EKF initialization, inertial position of the booster is approximated by a polynomial vector function with cubic terms,

$$\boldsymbol{r}_n=\boldsymbol{r}_1+\boldsymbol{v}_1(t_n-t_1)+\tfrac{1}{2}\boldsymbol{a}_1(t_n-t_1)^2+\tfrac{1}{6}\boldsymbol{b}_1(t_n-t_1)^3$$

where $\boldsymbol{r}_1$, $\boldsymbol{v}_1$, $\boldsymbol{a}_1$, and $\boldsymbol{b}_1$ are constant vectors representing inertial position, inertial velocity, total acceleration, and total jerk at the time t_1 of the first observation. Jerk terms are needed to extract certain EKF(12) state variables (to be discussed shortly). The polynomial model depends on the known elapsed time t_n-t_1 from the first observation. In contrast, template-based models must determine the elapsed time from launch to align the measurements with the template. The inertial position vector of the target is specified using the measurements

$$\boldsymbol{r}_n=\rho_n\boldsymbol{\lambda}_n+\boldsymbol{R}_n$$

Table 3 Nonlinear measurement models for EKF(12)

Angle-only sensor	Range-angle sensor
$\boldsymbol{y}_n=\boldsymbol{h}(\boldsymbol{r}_n)+\boldsymbol{\upsilon}_n,\qquad \boldsymbol{h}(\boldsymbol{r}_n)=\begin{bmatrix}\gamma(\boldsymbol{r}_n)\\ \psi(\boldsymbol{r}_n)\end{bmatrix}$	$\boldsymbol{y}_n=\boldsymbol{h}(\boldsymbol{r}_n)+\boldsymbol{\upsilon}_n,\qquad \boldsymbol{h}(\boldsymbol{r}_n)=\begin{bmatrix}\rho(\boldsymbol{r}_n)\\ \gamma(\boldsymbol{r}_n)\\ \psi(\boldsymbol{r}_n)\end{bmatrix}$
$R_n=E\left\{\boldsymbol{\upsilon}_n\boldsymbol{\upsilon}_n^T\right\}=\begin{bmatrix}E\left(\delta\gamma_n^2\right) & 0\\ 0 & E\left(\delta\psi_n^2\right)\end{bmatrix}$	$R_n=E\left\{\boldsymbol{\upsilon}_n\boldsymbol{\upsilon}_n^T\right\}=\begin{bmatrix}E\left(\delta\rho_n^2\right) & 0 & 0\\ 0 & E\left(\delta\gamma_n^2\right) & 0\\ 0 & 0 & E\left(\delta\psi_n^2\right)\end{bmatrix}$
$H_n(\boldsymbol{x}_n)=\dfrac{\partial\boldsymbol{h}_n}{\partial\boldsymbol{x}_n^T}=\begin{bmatrix}\dfrac{\partial\left(\gamma_n,\psi_n\right)}{\partial\boldsymbol{r}_n^T} & O_{2\times9}\end{bmatrix}$	$H_n(\boldsymbol{x}_n)=\dfrac{\partial\boldsymbol{h}_n}{\partial\boldsymbol{x}_n^T}=\begin{bmatrix}\dfrac{\partial(\rho_n,\gamma_n,\psi_n)}{\partial\boldsymbol{r}_n^T} & O_{3\times9}\end{bmatrix}$
$\dfrac{\partial(\gamma_n,\psi_n)}{\partial\boldsymbol{r}_n^T}=\begin{bmatrix}\dfrac{1}{\rho_n}\dfrac{\partial\boldsymbol{\lambda}_n^T}{\partial\gamma_n}\\ \dfrac{1}{\rho_n\cos^2\gamma_n}\dfrac{\partial\boldsymbol{\lambda}_n^T}{\partial\psi_n}\end{bmatrix}\Re(\boldsymbol{R}_n)$	$\dfrac{\partial(\rho_n,\gamma_n,\psi_n)}{\partial\boldsymbol{r}_n^T}=\begin{bmatrix}\boldsymbol{\lambda}_n^T\\ \dfrac{1}{\rho_n}\dfrac{\partial\boldsymbol{\lambda}_n^T}{\partial\gamma_n}\\ \dfrac{1}{\rho_n\cos^2\gamma_n}\dfrac{\partial\boldsymbol{\lambda}_n^T}{\partial\psi_n}\end{bmatrix}\Re(\boldsymbol{R}_n)$

After elimination of $\boldsymbol{r}_n$ from these equations, a set of linear equations may be derived,

$$\Psi \boldsymbol{X} = \boldsymbol{Y}$$

The extended state vector $\boldsymbol{X}$, the measurement vector $\boldsymbol{Y}$, and the matrix Ψ will depend on the data collected for initialization, as follows.

When N observations of $\boldsymbol{\lambda}_n$ are collected by a suite of angle-only sensors, the batch matrices may be expressed by

$$\boldsymbol{X}^T = \begin{bmatrix} \boldsymbol{r}_1^T & \boldsymbol{v}_1^T & \boldsymbol{a}_1^T & \boldsymbol{b}_1^T & \rho_1 & \rho_2 & \cdots & \rho_N \end{bmatrix}$$

$$\Psi = \begin{bmatrix} I_3 & O_3 & O_3 & O_3 & \Lambda_1 \\ I_3 & (t_2 - t_1) I_3 & \frac{1}{2}(t_2 - t_1)^2 I_3 & \frac{1}{6}(t_2 - t_1)^3 I_3 & \Lambda_2 \\ \vdots & \vdots & \vdots & \vdots & \vdots \\ I_3 & (t_N - t_1) I_3 & \frac{1}{2}(t_N - t_1)^2 I_3 & \frac{1}{6}(t_N - t_1)^3 I_3 & \Lambda_N \end{bmatrix}$$

$$\Lambda_n = [\boldsymbol{0}_3 \quad \cdots \quad -\boldsymbol{\lambda}_n \quad \cdots \quad \boldsymbol{0}_3]$$

$$\boldsymbol{Y}^T = \begin{bmatrix} \boldsymbol{R}_1^T & \boldsymbol{R}_2^T & \cdots & \boldsymbol{R}_N^T \end{bmatrix}$$

Elements of $\boldsymbol{X}$ include $\boldsymbol{r}_1, \boldsymbol{v}_1, \boldsymbol{a}_1, \boldsymbol{b}_1$, and N unknown distances $\rho_1, \rho_2, \ldots, \rho_N$, at the reporting times. The rectangular matrix Ψ has dimension $3N \times (N + 12)$ because $\boldsymbol{\lambda}_n$ is assigned to column $12 + n$ of the $3 \times (N + 12)$ matrix Λ_n. Because $\boldsymbol{X}$ has $N + 12$ unknowns and there are $3N$ observations of the components of $\boldsymbol{\lambda}_1, \boldsymbol{\lambda}_2, \ldots, \boldsymbol{\lambda}_N$, it is clear that $N \geq 6$ sets of independent observations are required for a properly conditioned solution. Nevertheless, an overdetermined solution, that is, $N \geq 12$, is recommended for smoothing measurement noise. (In reality, there are $2N$ independent angle observations because $|\boldsymbol{\lambda}_i| = 1$ and there are only 12 unknowns because each slant distance ρ_i may be determined from the trajectory solution. Nonetheless, the same requirement $N > 6$ is obtained.)

When N measurements of ρ_n and $\boldsymbol{\lambda}_n$ are collected by one range-angle sensor, the batch matrices may be simplified somewhat,

$$\boldsymbol{X}^T = \begin{bmatrix} \boldsymbol{r}_1^T & \boldsymbol{v}_1^T & \boldsymbol{a}_1^T & \boldsymbol{b}_1^T \end{bmatrix}$$

$$\Psi = \begin{bmatrix} I_3 & O_3 & O_3 & O_3 \\ I_3 & (t_2 - t_1) I_3 & \frac{1}{2}(t_2 - t_1)^2 I_3 & \frac{1}{6}(t_2 - t_1)^3 I_3 \\ \vdots & \vdots & \vdots & \vdots \\ I_3 & (t_N - t_1) I_3 & \frac{1}{2}(t_N - t_1)^2 I_3 & \frac{1}{6}(t_N - t_1)^3 I_3 \end{bmatrix}$$

$$\boldsymbol{Y}^T = \begin{bmatrix} \rho_1 \boldsymbol{\lambda}_1^T + \boldsymbol{R}_1^T & \rho_2 \boldsymbol{\lambda}_2^T + \boldsymbol{R}_2^T & \cdots & \rho_N \boldsymbol{\lambda}_N^T + \boldsymbol{R}_N^T \end{bmatrix}$$

Inasmuch as ρ_n is measured, $\boldsymbol{X}$ has only 12 unknowns because ρ_n is not included as a state variable.

For both types of sensors, an estimate $\hat{\boldsymbol{X}}$ is specified at t_1 by a least-squares solution,

$$\hat{\boldsymbol{X}} = K \boldsymbol{Y}, \qquad K = (\Psi^T \Psi)^{-1} \Psi^T$$

The covariance matrix P_B may be determined after linearization of the state equations about $\hat{\boldsymbol{X}}$ (Appendix B). After initialization of EKF(12) with the batch estimate and covariance matrix, the measurements are re processed using EKF(12). Because the batch initialization is based on an approximate trajectory model, it is expected that estimation accuracy will be improved.

Additional processing of $\hat{\boldsymbol{X}}$ and P_B is needed for EKF(12) initialization because $\hat{\boldsymbol{a}}_1$ and $\hat{\boldsymbol{b}}_1$ include gravity terms. For example, when aerodynamic accelerations are negligible, initial thrust acceleration and its derivative are specified after subtraction of the gravitational terms:

$$\hat{\boldsymbol{a}}_c(t_1) = \hat{\boldsymbol{a}}_1 - \boldsymbol{g}(\hat{\boldsymbol{r}}_1)$$

$$\frac{\mathrm{d}\hat{\boldsymbol{a}}_c(t_1)}{\mathrm{d}t} = \hat{\boldsymbol{b}}_1 - \frac{\mathrm{d}\boldsymbol{g}(\hat{\boldsymbol{r}}_1)}{\mathrm{d}t} = \hat{\boldsymbol{b}}_1 - \Gamma_1 \hat{\boldsymbol{v}}_1, \qquad \Gamma_1 = \Gamma(\hat{\boldsymbol{r}}_1)$$

The total angular velocity may be determined from the kinematic identity

$$\hat{\boldsymbol{\varpi}}(t_1) + \hat{\boldsymbol{\omega}}(t_1) = \frac{1}{a_c^2} \left[\hat{\boldsymbol{a}}_c(t_1) \times \frac{\mathrm{d}\hat{\boldsymbol{a}}_c(t_1)}{\mathrm{d}t} \right]$$

An estimate of the Markov angular velocity may be determined after subtraction of $\hat{\boldsymbol{\omega}}(t_1)$,

$$\hat{\boldsymbol{\omega}}(t_1) = \left(1/a_c^2\right)[\hat{\boldsymbol{a}}_1 - \boldsymbol{g}(\hat{\boldsymbol{r}}_1)] \times [\hat{\boldsymbol{b}}_1 - \Gamma_1 \hat{\boldsymbol{v}}_1] - \left(\hat{\boldsymbol{u}}_1 / \hat{u}_1^2\right) \times \hat{\boldsymbol{a}}_1$$

Although $\hat{\boldsymbol{a}}_c(t_1)$ and $\hat{\boldsymbol{\varpi}}(t_1)$ are nonlinear functions of the other state variables, the errors in the estimates may be approximated by linear functions of the errors in the batch estimates,

$$\delta \hat{\boldsymbol{a}}_c(t_1) = \delta \hat{\boldsymbol{a}}_1 - \Gamma(\hat{\boldsymbol{r}}_1) \delta \hat{\boldsymbol{r}}_1$$

$$\delta \hat{\boldsymbol{\varpi}}(t_1) = S_r \delta \hat{\boldsymbol{r}}(t_1) + S_v \delta \hat{\boldsymbol{v}}(t_1) + S_a \delta \hat{\boldsymbol{a}}(t_1) + S_b \delta \hat{\boldsymbol{b}}(t_1)$$

$$S_r \cong \left(1/a_c^2\right) \Omega(\hat{\boldsymbol{b}}_1 - \Gamma_1 \hat{\boldsymbol{v}}_1) \Gamma_1 + \left(2/a_c^4\right) \Omega(\hat{\boldsymbol{a}}_c)(\hat{\boldsymbol{b}}_1 - \Gamma_1 \hat{\boldsymbol{v}}_1) \hat{\boldsymbol{a}}_c^T \Gamma_1 - \left(1/u_1^2\right) \left[\Omega(\hat{\boldsymbol{a}}_1) - \left(2/u_1^2\right) \hat{\boldsymbol{u}}_1 \hat{\boldsymbol{u}}_1^T \right] \Omega(\boldsymbol{\omega}_e) + \text{hot}$$

$$S_v = -\left(1/a_c^2\right) \Omega(\hat{\boldsymbol{a}}_c) \Gamma_1 + \left(1/u_1^2\right) \Omega(\hat{\boldsymbol{a}}_1) \left[I_3 - \left(2/u_1^2\right) \hat{\boldsymbol{u}}_1 \hat{\boldsymbol{u}}_1^T \right]$$

$$S_a = -\left(1/a_c^2\right) \Omega(\hat{\boldsymbol{b}}_1 - \Gamma_1 \hat{\boldsymbol{v}}_1) - \left(2/a_c^4\right) \Omega(\hat{\boldsymbol{a}}_c) \times (\hat{\boldsymbol{b}}_1 - \Gamma_1 \hat{\boldsymbol{v}}_1) \hat{\boldsymbol{a}}_c^T - \left(1/u_1^2\right) \Omega(\hat{\boldsymbol{u}}_1)$$

$$S_b = \left(1/a_c^2\right) \Omega(\hat{\boldsymbol{a}}_c)$$

The initial covariance matrix $P(t_1)$ is derived from the batch covariance matrix $P_B(t_1)$,

$$P(t_1) = S P_B S^T, \qquad S = \begin{bmatrix} I_3 & O_3 & O_3 & O_3 \\ O_3 & I_3 & O_3 & O_3 \\ -\Gamma_1 & O_3 & I_3 & O_3 \\ S_r & S_v & S_a & S_b \end{bmatrix}$$

V. Iteration of the Estimates with Acceleration Constraints

For each reported position measurement, state estimates and covariances of EKF(12) and EKF(6) are iterated before IMM estimation (Table 4). By the use of superscripts to indicate the iteration number, the EKF(12) iteration process begins ($i = 0$) with the prior estimate and covariance,

$$\hat{\boldsymbol{x}}_n^{(0)} = \bar{\boldsymbol{x}}_n, \qquad P_n^{(0)} = M_n$$

In the prior covariance matrix M_n, errors in position states (which are directly observable from the measurements) are correlated with errors in velocity, acceleration, and angular rate. These correlations enable correction of velocity, acceleration, and angular rate errors with position measurements through the filter gain matrix. Similar considerations apply to EKF(6).

The first iteration ($i = 1$) is the conventional EKF. Because $\varepsilon_n^{(1)}$ is not used to update $P_n^{(1)}$, the residuals covariance $N_n^{(1)}$ is derived from a linear model (Table 4). Nonlinear effects usually cause differences between $N_n^{(1)}$ and the actual statistics of the residuals. Consequently, $P_n^{(1)}$ may not accurately represent the statistics of errors in the estimates. Process noise can be tuned to improve agreement of the statistics of the errors in the estimates and the statistics predicted by the covariance matrix, that is, covariance fidelity.

Alternatively, iteration of the estimate and covariance may improve covariance fidelity, provided that the states are sufficiently observable.[13] For $i > 1$, the additional term in $\varepsilon_n^{(i)}$ improves the accuracy of the iterated estimate $\hat{\boldsymbol{x}}_n^{(i)}$ compared to $\hat{\boldsymbol{x}}_n^{(1)}$. Similarly, $P_n^{(i)}$ is improved compared to $P_n^{(1)}$ because $H(\boldsymbol{x}_n)$ is evaluated with the

Table 4 Iterated updates of boost and Keplerian estimates ($0 <= i <= 3$)

Boost EKF(12)	Keplerian EKF(6)
$\hat{\boldsymbol{x}}_n^{(0)} = \bar{\boldsymbol{x}}_n, \qquad P_n^{(0)} = M_n$	$\hat{\boldsymbol{\xi}}_n^{(0)} = \bar{\boldsymbol{\xi}}_n, \qquad \Xi_n^{(0)} = \bar{\Xi}_n$
$K_n^{(i)} = M_n H\left(\hat{\boldsymbol{x}}_n^{(i)}\right)^T \left(N_n^{(i)}\right)^{-1}$	$K_n^{(i)} = \bar{\Xi}_n H\left(\hat{\boldsymbol{\xi}}_n^{(i)}\right)^T \left(D_n^{(i)}\right)^{-1}$
$N_n^{(i)} = H\left(\hat{\boldsymbol{x}}_n^{(i)}\right) M_n H\left(\hat{\boldsymbol{x}}_n^{(i)}\right)^T + R_n$	$D_n^{(i)} = H\left(\hat{\boldsymbol{\xi}}_n^{(i)}\right) \bar{\Xi}_n H\left(\hat{\boldsymbol{\xi}}_n^{(i)}\right)^T + R_n$
$P_n^{(i+1)} = K_n^{(i)} R_n \left(K_n^{(i)}\right)^T + \left[I_{12} - K_n^{(i)} H\left(\hat{\boldsymbol{x}}_n^{(i)}\right)\right] M_n \left[I_{12} - K_n^{(i)} H\left(\hat{\boldsymbol{x}}_n^{(i)}\right)\right]^T$	$\Xi_n^{(i+1)} = K_n^{(i)} R_n \left(K_n^{(i)}\right)^T + \left[I_{12} - K_n^{(i)} H\left(\hat{\boldsymbol{\xi}}_n^{(i)}\right)\right] \bar{\Xi}_n \left[I_{12} - K_n^{(i)} H\left(\hat{\boldsymbol{\xi}}_n^{(i)}\right)\right]^T$
$\hat{\boldsymbol{x}}_n^{(i+1)} = \bar{\boldsymbol{x}}_n + K_n^{(i)} \boldsymbol{\varepsilon}_n^{(i)}$	$\hat{\boldsymbol{\xi}}_n^{(i+1)} = \bar{\boldsymbol{\xi}}_n + K_n^{(i)} \boldsymbol{\delta}_n^{(i)}$
$\boldsymbol{\varepsilon}_n^{(i)} = \boldsymbol{y}_n - \boldsymbol{h}\left(\hat{\boldsymbol{x}}_n^{(i)}\right) - H\left(\hat{\boldsymbol{x}}_n^{(i)}\right)\left(\bar{\boldsymbol{x}}_n - \hat{\boldsymbol{x}}_n^{(i)}\right)$	$\boldsymbol{\delta}_n^{(i)} = \boldsymbol{y}_n - \boldsymbol{h}\left(\hat{\boldsymbol{\xi}}_n^{(i)}\right) - H\left(\hat{\boldsymbol{\xi}}_n^{(i)}\right)\left(\bar{\boldsymbol{\xi}}_n - \hat{\boldsymbol{\xi}}_n^{(i)}\right)$

latest iterate $\hat{\boldsymbol{x}}_n^{(i)}$. During the iteration process, the prior estimates and covariances are not iterated and the same measurement data $\boldsymbol{y}_n$ and noise matrix R_n are used for updating EKF(12) and EKF(6). Performance analysis results (to be discussed shortly) suggest that two or three iterations are sufficient.

Poor measurements can sometimes cause wild estimates of $\boldsymbol{a}_c$. These problems can be aggravated by forward prediction to the next update. For long prediction intervals, predictions of thrust acceleration magnitude can become unbounded. For constant U, it may be shown that

$$a_c(t) = \frac{a_c(t_0)}{1 - (t - t_0)/T_B}, \qquad T_B = \frac{U}{a_c(t_0)}$$

Although the mathematical singularity at $t = t_0 + T_B$ (corresponding to zero mass) never occurs, a_c can, nonetheless, become unrealistically large.

These problems can be avoided with constraints on the magnitude and orientation of $\boldsymbol{a}_c$. Constraints on thrust acceleration magnitude preclude unbounded accelerations,

$$a_{\min} \le |\boldsymbol{a}_c| \le a_{\max}(v)$$

Numerical values $a_{\min} = 2.5g$ and $a_{\max} = 10$–$15g$ are recommended for typical intercontinental ballistic missiles (ICBMs), although a velocity-dependent constraint $a_{\max}(v)$ is an effective technique for anticipation of burnout events. Orientation constraints are enforced when the angle α between $\boldsymbol{a}_c$ and $\boldsymbol{u}$ exceeds a certain threshold $\alpha_{\max}$. For $\alpha \ge \alpha_{\max} (= 60 \text{ deg})$, the unit thrust vector $\boldsymbol{e}$ is constrained to the instantaneous plane defined by $\boldsymbol{r}$ and $\boldsymbol{u}$,

$$\boldsymbol{e} = \frac{\boldsymbol{a}_c}{|\boldsymbol{a}_c|} = \cos(\alpha_{\max})\left(\frac{\boldsymbol{u}}{u}\right) + \sin(\alpha_{\max})\frac{\boldsymbol{u} \times \boldsymbol{n}}{|\boldsymbol{u} \times \boldsymbol{n}|}, \qquad \boldsymbol{n} = \frac{\boldsymbol{r} \times \boldsymbol{u}}{|\boldsymbol{r} \times \boldsymbol{u}|}$$

During long predictions, $\alpha_{\max} = 0$ is recommended until more measurement data is available.

VI. Multiple Model Estimation

Staging and thrust termination events may be handled using an IMM technique.[15–19] At any time t_n, the state of the system is described by a boost hypothesis B_n or by a Keplerian hypothesis K_n that corresponds to the situations when the booster coasts after a staging event or terminates thrust at burnout.

A composite estimate $\hat{\boldsymbol{x}}_n^*$ is the expected value of the state and P_n^* is its error covariance, given the set of all measurements $Y_n = \{\boldsymbol{y}_n \ \cdots \ \boldsymbol{y}_0\}$ that includes the most recent measurement $\boldsymbol{y}_n$. Here $\hat{\boldsymbol{x}}_n^*$ and P_n^* are determined from the iterated estimates and covariances $\hat{\boldsymbol{x}}_n$ and P_n of EKF(12), iterated estimates and covariances $\hat{\boldsymbol{\xi}}_n$ and Ξ_n of EKF(6), and certain statistical weights $\hat{\beta}_n$ and $\hat{\kappa}_n$. (Refer to Table 5 where superscripts have been suppressed to simplify notation.) The normalization constant c is selected such that $\hat{\beta}_n + \hat{\kappa}_n = 1$ (to be discussed shortly). (The EKF(6) state vector and covariance are augmented with zeros to increase dimensionality from 6 to 12 to fuse with the EKF(12) state vector and covariance. Zeros are appropriate for the Keplerian model because the thrust acceleration and Markov angular velocity terms are zero with zero uncertainties.)

Table 5 IMM blending

State and covariance	Statistical weights
$\hat{\boldsymbol{x}}_n^* = \hat{\beta}_n \hat{\boldsymbol{x}}_n + \hat{\kappa}_n \hat{\boldsymbol{\xi}}_n$	$\hat{\beta}_n = \dfrac{\exp\left[-\frac{1}{2}\boldsymbol{\varepsilon}_n^T N_n^{-1} \boldsymbol{\varepsilon}_n\right]}{(2\pi)^{\frac{3}{2}} c\sqrt{\lvert N_n \rvert}} \bar{\beta}_n$
$P_n^* = \hat{\beta}_n\left[P_n + \left(\hat{\boldsymbol{x}}_n - \hat{\boldsymbol{x}}_n^*\right)\left(\hat{\boldsymbol{x}}_n - \hat{\boldsymbol{x}}_n^*\right)^T\right] + \hat{\kappa}_n\left[\Xi_n + \left(\hat{\boldsymbol{\xi}}_n - \hat{\boldsymbol{x}}_n^*\right)\left(\hat{\boldsymbol{\xi}}_n - \hat{\boldsymbol{x}}_n^*\right)^T\right]$	$\hat{\kappa}_n = \dfrac{\exp\left[-\frac{1}{2}\boldsymbol{\delta}_n^T D_n^{-1} \boldsymbol{\delta}_n\right]}{(2\pi)^{\frac{3}{2}} c\sqrt{\lvert D_n \rvert}} \bar{\kappa}_n$

Posterior probabilities that B_n and K_n correctly represent the current state of the system, conditioned on Y_n, may be determined using Bayes's rule,

$$\hat{\beta}_n = p(B_n|Y_n) = [p(\boldsymbol{y}_n|B_n)p(B_n|Y_{n-1})]/p(Y_n)$$

$$\hat{\kappa}_n = p(K_n|Y_n) = [p(\boldsymbol{y}_n|K_n)p(K_n|Y_{n-1})]/p(Y_n)$$

Conditional measurement probabilities are expressed by likelihood functions involving the iterated residuals $\boldsymbol{\varepsilon}_n$ and $\boldsymbol{\delta}_n$ and the residuals covariance matrices N_n and D_n (superscripts omitted),

$$p(\boldsymbol{y}_n|B_n) = \frac{\exp\left[-\frac{1}{2}\boldsymbol{\varepsilon}_n^T N_n^{-1} \boldsymbol{\varepsilon}_n\right]}{(2\pi)^{\frac{3}{2}}\sqrt{|N_n|}}$$

$$p(\boldsymbol{y}_n|K_n) = \frac{\exp\left[-\frac{1}{2}\boldsymbol{\delta}_n^T D_n^{-1} \boldsymbol{\delta}_n\right]}{(2\pi)^{\frac{3}{2}}\sqrt{|D_n|}}$$

Prior probabilities $\bar{\beta}_n$ and $\bar{\kappa}_n$ are conditioned on the set Y_{n-1} of all previous measurements,

$$\bar{\beta}_n = p(B_n|Y_{n-1}), \qquad \bar{\kappa}_n = p(K_n|Y_{n-1})$$

It then follows that

$$p(Y_n) = p(\boldsymbol{y}_n|B_n)\bar{\beta}_n + p(\boldsymbol{y}_n|K_n)\bar{\kappa}_n = c$$

Prior probabilities $\bar{\beta}_n$ and $\bar{\kappa}_n$ reflect the complete history of all previous estimates, covariances, and measurements Y_{n-1}. After $\hat{\beta}_n$ and $\hat{\kappa}_n$ are updated with the most recent information, probabilities are predicted to the next update using a Markov state-transition matrix W:

$$\begin{bmatrix}\bar{\beta}_{n+1} \\ \bar{\kappa}_{n+1}\end{bmatrix} = W \begin{bmatrix}\hat{\beta}_n \\ \hat{\kappa}_n\end{bmatrix}, \qquad W = \begin{bmatrix}p(B_{n+1}|B_n) & p(B_{n+1}|K_n) \\ p(K_{n+1}|B_n) & p(K_{n+1}|K_n)\end{bmatrix}$$

Elements of W are conditional probabilities, and each column must sum to unity. For example, $p(B_{n+1}|B_n)$ is the probability that a

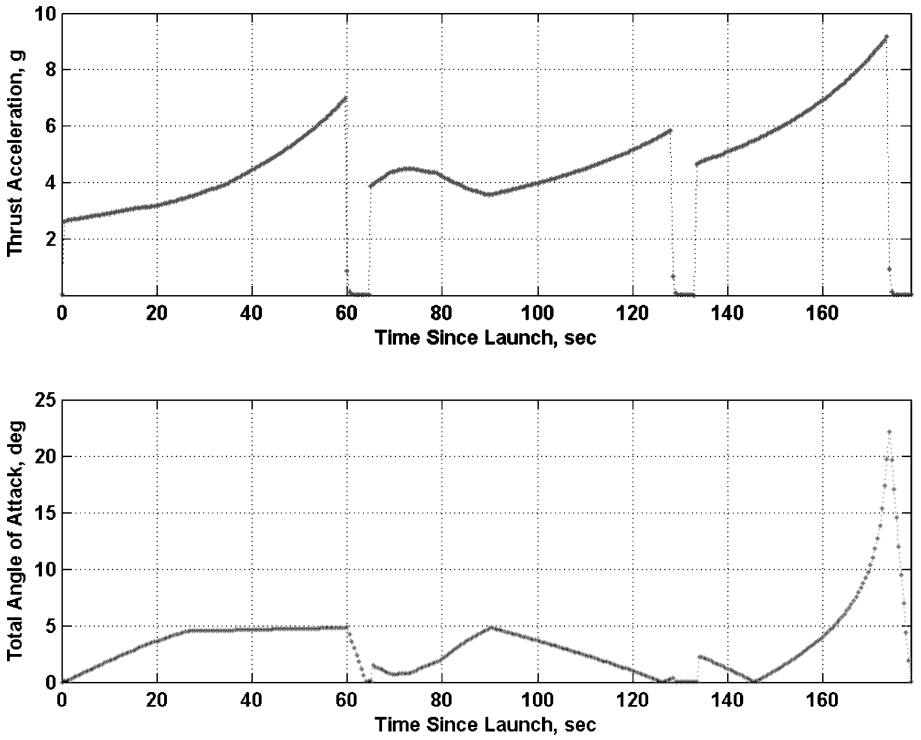

Fig. 2 Thrust acceleration and total angle of attack between thrust acceleration and Earth-relative velocity for a representative three-stage ICBM boost trajectory.

Table 6 Markov state transition probabilities

Case	Boost state B_n at t_n	Keplerian state K_n at t_n
Boost state B_{n+1} at t_{n+1}	$p(B_{n+1}\|B_n)=0.9$	$p(K_{n+1}\|B_n)=0.1$
Keplerian state K_{n+1} at t_{n+1}	$p(B_{n+1}\|K_n)=0.1$	$p(K_{n+1}\|K_n)=0.9$

transition occurs from a boost state B_n at t_n to another boost state B_{n+1} at t_{n+1} and similarly for the other elements of W.

Numerical values of the transition probabilities are constants that are selected as part of the design process (Table 6). Performance results (not reported here) are not sensitive to reasonable values of the probabilities. Other precautions assure that the algorithm is not prejudiced by prior information about the timing of staging events and the number of missile stages. For example, the numerical values $p(B_{n+1}|K_n)=0$ and $p(K_{n+1}|K_n)=1$ are not assigned because these values would indicate an irreversible transition from B_n to K_{n+1}, that is, a single-stage missile. Similarly, variable transition probabilities are not used because time histories would probably be based on prior information.

State estimates and covariances are predicted to the next IMM update, as follows. Initial conditions $\hat{\boldsymbol{x}}_n^*$ and P_n^* are input to both the EKF(12) and EKF(6) prediction models (Fig. 1). This simplification reduces the computational complexity of the IMM algorithm because a detailed geneaology of all past estimates and hypotheses is not required.

VII. Performance Analysis

EKF(12) performance is determined by Monte Carlo simulation of the filtering process with nonlinear truth models of the booster trajectory and sensors. A representative three-stage ICBM is simulated with nonlinear guidance, control, aerodynamics, and thrust actuation models. Steering maneuvers are constrained by total angle of attack during stages 1 and 2, and much larger angles are permitted during stage 3 to close the Lambert guidance loop (Fig. 2). Stereo coverage of the boost phase is provided by two geosynchronous satellites, separated in longitude by 90°. Sensors report angle-only measurements that are corrupted by zero-mean Gaussian random variables with cross-range position uncertainties of approximately 350 m. A single ground-based sensor, offset by approximately 200 km from the boost trajectory plane, reports three-dimensional position measurements that are an order of magnitude more accurate than the spaceborne sensors. Measurement updates occur every 1–2 s for both sensors.

For angle-only sensors, EKF(12) performance depends on the acceleration process noise q_a, the Markov time constant τ, the Markov angular velocity process noise q_ϖ, and the number of EKF iterations. Baseline values of these four parameters (Table 2) were selected to achieve close agreement of the Monte Carlo error statistics and the error statistics predicted by the covariances. One performance metric is the covariance fidelity ratio of the rss Monte Carlo errors to the rss filter covariance errors at a specified spherical error probability (SEP) level, for example, 97%. Fidelity ratios for position, velocity, and thrust acceleration are time-averaged over the last 20 time points before burnout to dampen statistical fluctuations associated with small Monte Carlo sample size (100 trials). Ensemble averages show that each ratio has different sensitivity to the tuning parameters (Fig. 3). Position, velocity, and thrust acceleration fidelity ratios show different sensitivities to the tuning parameters. Statistics are determined using stereo angle-only sensors. Simulation results show that covariance fidelity ratios are closest to unity for cases 1, 8, and 9, although small Monte Carlo sample size (100 trials) and short time in track (under 500 s) probably obscure progressive improvement with an increasing number of EKF iterations. It is found that three Markov angular velocity states absorb some process noise, thereby reducing the q_a value recommended in a previous publication.[10]

Satisfactory IMM performance demands high probability that boost model predictions can be differentiated from the Keplerian model predictions. Model separability depends on the position mismatch that accumulates during the time interval T between measurements compared to the position measurement uncertainty σ_P. The position mismatch is caused by the acceleration mismatch $\Delta\boldsymbol{a}$ between models. For example, the separation probability may be modeled by a χ^2 cumulative distribution with three degrees of freedom, such that

$$\chi^2 = \left(\tfrac{1}{2}|\Delta\boldsymbol{a}|T^2/\sigma_P\right)^2$$

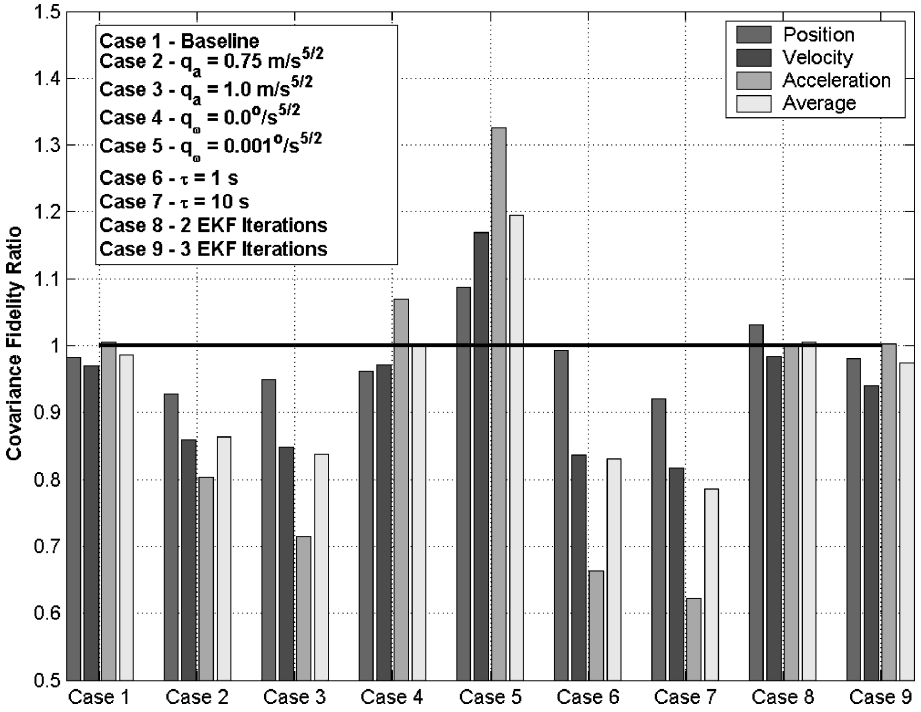

Fig. 3 Covariance fidelity ratio depends on four EKF(12) tuning parameters: Baseline $q_a = 0.5$ m/s$^{5/2}$, $q_\omega = 0.01°/s^{5/2}$, and $\tau = 100$ s, 1 iteration.

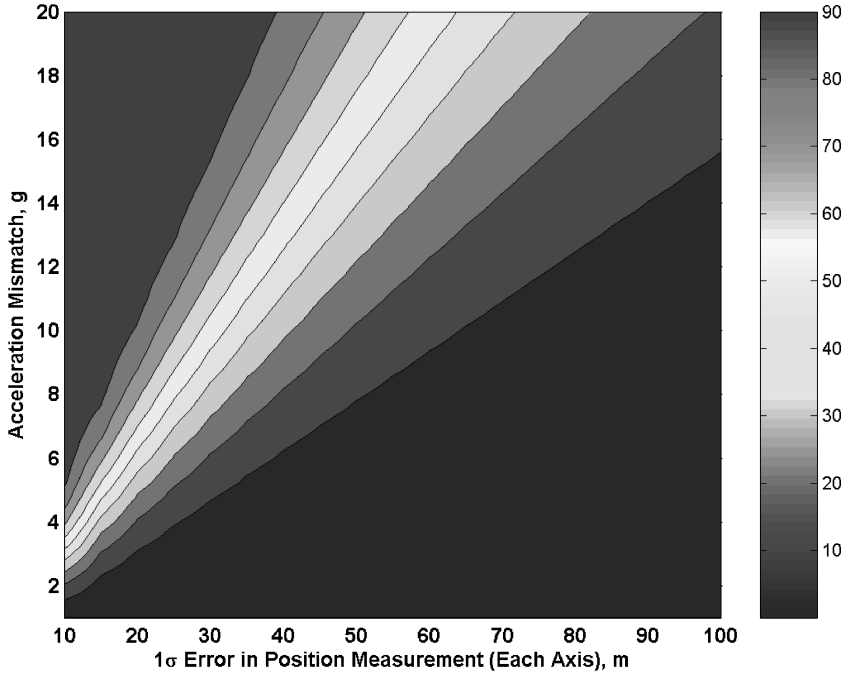

Fig. 4 Probability of IMM separation increases as acceleration mismatch increases and as position measurement errors decrease.

Separation probabilities increase as σ_P decreases and as $|\Delta \boldsymbol{a}|$ increases (Fig. 4). In Fig. 4, note that probabilities are determined by a χ^2 distribution with three degrees of freedom and with measurement updates at 1-s intervals. Results are applicable to stereo angle-only sensors and range-angle sensors. For small T values, a very accurate sensor, for example, a radar, is clearly preferred. For a specified σ_P value, staging and burnout events are more easily detected because $|\Delta \boldsymbol{a}|$ is large, but booster reignition after a staging event is more difficult to detect because $|\Delta \boldsymbol{a}|$ is small.

With an accurate range-angle sensor, the IMM filter successfully tracks during powered flight, through two staging events, and through the final burnout event (Figs. 5 and 6). Note from Fig. 5 that minimum thrust acceleration does not exceed 2.5 g for boost EKF(12). IMM thrust acceleration magnitude blends the responses of boost EKF(12) and Keplerian EKF(6) using corresponding statistical weights. Statistical weights indicate detection of the two staging events and the final burnout event. It was found that EKF(12) can detect and respond to the three burnout events, but EKF(12) response is sluggish to booster reignition following short coast segments after the two staging events. With a minimum thrust acceleration of 2.5g, IMM response is dramatically improved, as is evident in the responsive IMM probabilities. The minimum acceleration constraint enhances the separability of the boost and Keplerian models at the booster reignition events. The IMM filter exhibits small acceleration errors during the two coast segments and shortly after burnout

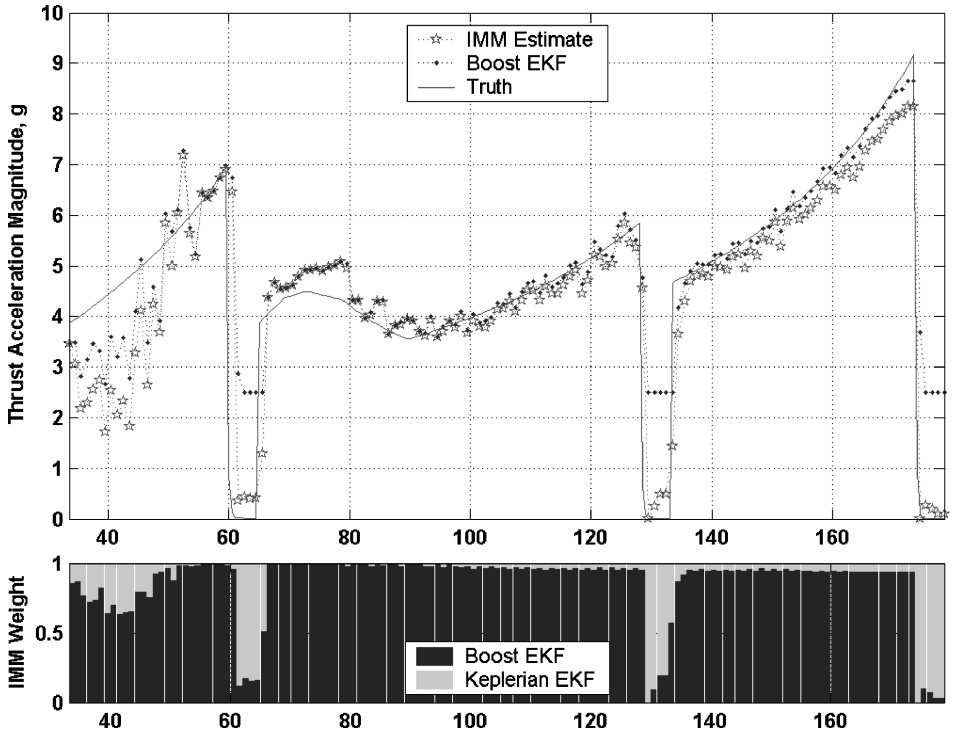

Fig. 5 Estimation of thrust acceleration magnitude using IMM filter with range-angle sensor.

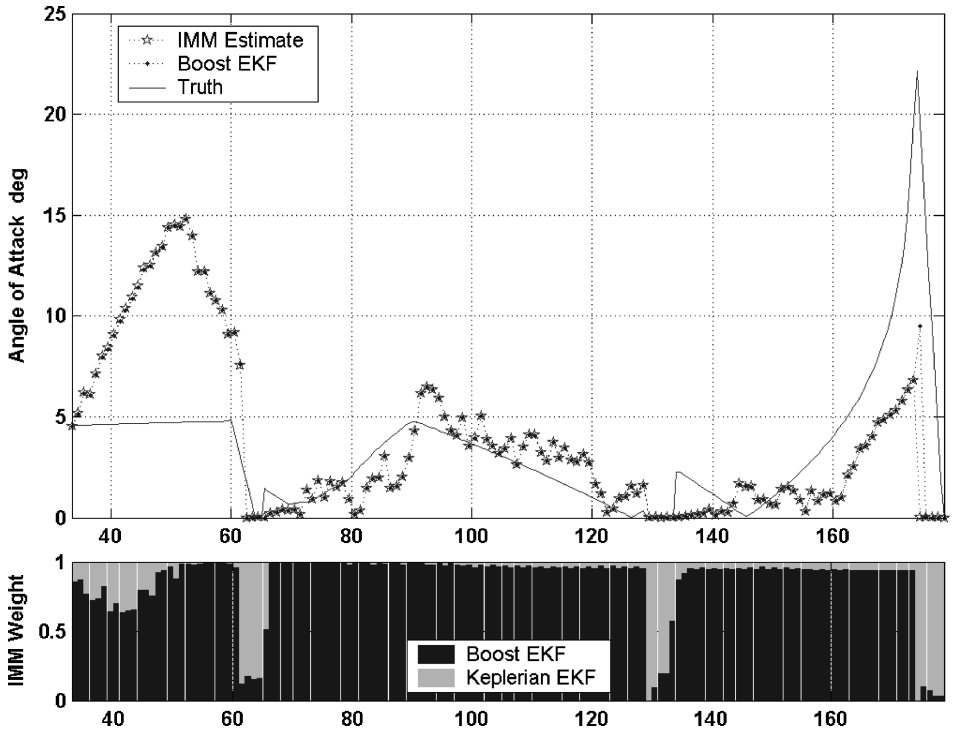

Fig. 6 Estimation of booster orientation using IMM filter with range-angle sensor.

(because 2.5 g is blended with 0 g), but these errors are quickly corrected.

VIII. Conclusions

A 12-state, iterated nonlinear recursive filter was formulated for boost trajectory estimation and prediction. The recursive filter is initialized with state and covariance estimates from a polynomial batch filter. Staging and burnout events are handled with an IMM technique that statistically blends boost filter estimates with those of a six-state Keplerian filter. Prior trajectory information (such as a booster template) is not needed because this physics-based algorithm can adapt using measurements from a suite of angle-only sensors, from one or more range-angle sensors, or from both types of sensors in a data fusion mode.

A new contribution of this article is a boost prediction model that includes terms that model the nonlinear growth of thrust acceleration magnitude caused by propellant depletion and variations in thrust orientation associated with gravity-turn maneuvers and steering

maneuvers at constant or variable angles of attack. A first-order Markov process absorbs angular velocities that are not modeled by gravity turns or accelerated turns at constant angle of attack. The measurements are used to update filter the initial conditions periodically as actual flight conditions change.

Constraints are enforced on the magnitude and direction of thrust acceleration estimates and predictions. Because poor measurements can cause wild acceleration estimates, these constraints allow the filter to recover when better information becomes available. Constraints are also useful during long prediction intervals without measurements because thrust acceleration magnitude could become unrealistically large.

An IMM technique blends boost and Keplerian filter estimates with statistical weights that depend on the statistics of the measurement residuals. Satisfactory IMM tracking performance and reliable detection of staging and burnout events demand accurate position measurements (such as those provided by radars) and a sufficiently large acceleration mismatch between the boost and Keplerian models. Constraints on minimum thrust acceleration also enhance model separability.

EKF(12) parameters were tuned by Monte Carlo simulations with the nonlinear truth models for the booster and sensors. Two process noise parameters, the Markov time constant and the number of EKF(12) iterations, were selected to achieve agreement of filter error statistics and covariance predictions. Generally, two or three iterations are recommended for good performance. Numerical values of the tuning parameters are not sensitive to the booster acceleration profile.

The IMM algorithm is applicable across a broad spectrum of missile defense applications. EKF(12) has been successfully simulated with infrared and radar sensors. The prediction model has been applied (elsewhere) to the prediction of aimpoints for boost phase intercept, to launch point retrodiction, and to burnout and postboost prediction for cuing downrange sensors. Improved accuracies of the burnout state estimate and of burnout covariances will mitigate requirements on the size of cued search volumes for downrange missile defense sensors.

Appendix A: EKF Boost Dynamics Matrix

Elements of the linearized dynamics matrix F are derived by partial differentiations of the following equations of motion with respect to the state variables:

$$\boldsymbol{b} \equiv \frac{\mathrm{d}\boldsymbol{a}_c}{\mathrm{d}t} = \frac{a}{U}\boldsymbol{a}_c + \Omega(\boldsymbol{\omega} + \boldsymbol{\varpi})\boldsymbol{a}_c$$

$$\boldsymbol{\omega} = \frac{1}{u^2}\Omega(\boldsymbol{u})[\boldsymbol{g}(\boldsymbol{r}) + \boldsymbol{a}_c], \qquad \boldsymbol{u} = \boldsymbol{v} - \Omega(\boldsymbol{\omega}_e)\boldsymbol{r}$$

where $\Omega(*)$ is the 3×3 skew-symmetric cross product matrix. After permutation of the cross products, a second set of equivalent identities is generated,

$$\boldsymbol{b} = (a/U)\boldsymbol{a}_c - \Omega(\boldsymbol{a}_c)(\boldsymbol{\omega} + \boldsymbol{\varpi}), \qquad \boldsymbol{\omega} = -(1/u^2)\Omega(\boldsymbol{g} + \boldsymbol{a}_c)\boldsymbol{u}$$

Partial derivatives of these identities are organized into four submatrices contained in F,

$$A = \frac{\partial \boldsymbol{b}}{\partial \boldsymbol{r}^T}, \qquad B = \frac{\partial \boldsymbol{b}}{\partial \boldsymbol{v}^T}, \qquad C = \frac{\partial \boldsymbol{b}}{\partial \boldsymbol{a}_c^T}, \qquad D = \frac{\partial \boldsymbol{b}}{\partial \boldsymbol{\varpi}^T}$$

Using the preceding identities, partial derivatives of $\boldsymbol{b}$ with respect to position, velocity, thrust acceleration, and angular velocity may be expressed by

$$A = -\Omega(\boldsymbol{a}_c)\frac{\partial \boldsymbol{\omega}}{\partial \boldsymbol{r}^T}, \qquad B = -\Omega(\boldsymbol{a}_c)\frac{\partial \boldsymbol{\omega}}{\partial \boldsymbol{v}^T}, \qquad D = -\Omega(\boldsymbol{a}_c)$$

$$C = \frac{1}{U}\frac{\partial}{\partial \boldsymbol{a}_c^T}(a\boldsymbol{a}_c) + \Omega(\boldsymbol{\omega} + \boldsymbol{\varpi}) - \Omega(\boldsymbol{a}_c)\frac{\partial \boldsymbol{\omega}}{\partial \boldsymbol{a}_c^T}$$

Partial derivatives of $\boldsymbol{\omega}$ may be expressed by

$$\frac{\partial \boldsymbol{\omega}}{\partial \boldsymbol{r}^T} = \frac{1}{u^2}\left[\Omega(\boldsymbol{u})\frac{\partial \boldsymbol{g}}{\partial \boldsymbol{r}^T} - \Omega(\boldsymbol{g} + \boldsymbol{a}_c)\frac{\partial \boldsymbol{u}}{\partial \boldsymbol{r}^T}\right] + \frac{2}{u^3}\Omega(\boldsymbol{g} + \boldsymbol{a}_c)\boldsymbol{u}\frac{\partial u}{\partial \boldsymbol{r}^T}$$

$$\frac{\partial \boldsymbol{\omega}}{\partial \boldsymbol{v}^T} = \frac{-1}{u^2}\Omega(\boldsymbol{g} + \boldsymbol{a}_c)\frac{\partial \boldsymbol{u}}{\partial \boldsymbol{v}^T} + \frac{2}{u^3}\Omega(\boldsymbol{g} + \boldsymbol{a}_c)\boldsymbol{u}\frac{\partial u}{\partial \boldsymbol{v}^T}$$

$$\frac{\partial \boldsymbol{\omega}}{\partial \boldsymbol{a}_c^T} = \frac{1}{u^2}\Omega(\boldsymbol{u})$$

Partial derivatives of the Earth-relative velocity vector and its magnitude may be expressed by

$$\frac{\partial \boldsymbol{u}}{\partial \boldsymbol{r}^T} = -\Omega(\boldsymbol{\omega}_e), \qquad \frac{\partial u}{\partial \boldsymbol{r}^T} = \frac{-1}{u}\boldsymbol{u}^T\Omega^T(\boldsymbol{\omega}_e)$$

$$\frac{\partial \boldsymbol{u}}{\partial \boldsymbol{v}^T} = I_3, \qquad \frac{\partial u}{\partial \boldsymbol{v}^T} = \frac{1}{u}\boldsymbol{u}^T$$

When terms are collected, it follows that

$$A = -(1/u^2)\Omega(\boldsymbol{a}_c)\left\{\Omega(\boldsymbol{u})\Gamma(\boldsymbol{r}) + \Omega(\boldsymbol{a}_c + \boldsymbol{g})\left[\Omega(\boldsymbol{\omega}_e) - (2/u^2)\boldsymbol{u}\boldsymbol{u}^T\Omega^T(\boldsymbol{\omega}_e)\right]\right\}$$

$$B = (1/u^2)\Omega(\boldsymbol{a}_c)\Omega(\boldsymbol{a}_c + \boldsymbol{g})\left[I_3 - (2/u^2)\boldsymbol{u}\boldsymbol{u}^T\right]$$

$$C = (1/aU)\left(a^2 I_3 + \boldsymbol{a}_c\boldsymbol{a}_c^T\right) + \Omega(\boldsymbol{\omega} + \boldsymbol{\varpi}) - (1/u^2)\Omega(\boldsymbol{a}_c)\Omega(\boldsymbol{u})$$

$$D = -\Omega(\boldsymbol{a}_c)$$

Appendix B: Batch Covariance Matrix for Angle-Only Sensors

For angle-only sensors, the state equations of the polynomial batch filter may be linearized about the least-squares solution $\hat{\boldsymbol{X}}$,

$$\Psi\delta\hat{\boldsymbol{X}} + \delta\Psi\hat{\boldsymbol{X}} = \delta\boldsymbol{Y}$$

$$\delta\hat{\boldsymbol{X}}^T = \begin{bmatrix}\delta\hat{\boldsymbol{r}}_1^T & \delta\hat{\boldsymbol{v}}_1^T & \delta\hat{\boldsymbol{a}}_1^T & \delta\hat{\boldsymbol{b}}_1^T & \delta\hat{\rho}_1 & \delta\hat{\rho}_2 & \cdots & \delta\hat{\rho}_N\end{bmatrix}$$

$$\delta\Psi = \begin{bmatrix} O_3 & O_3 & O_3 & \delta\Lambda_1 \\ O_3 & O_3 & O_3 & \delta\Lambda_2 \\ \vdots & \vdots & \vdots & \vdots \\ O_3 & O_3 & O_3 & \delta\Lambda_N \end{bmatrix}$$

$$\delta\Lambda_n = [\boldsymbol{0}_3 \quad \cdots \quad -\delta\boldsymbol{\lambda}_n \quad \cdots \quad \boldsymbol{0}_3]$$

$$\delta\boldsymbol{Y}^T = \begin{bmatrix}\delta\boldsymbol{R}_1^T & \delta\boldsymbol{R}_2^T & \cdots & \delta\boldsymbol{R}_n^T\end{bmatrix}$$

where $\delta\boldsymbol{\lambda}_n$is the error in the unit LOS vector and $\delta\boldsymbol{R}_n$ is the geolocation error in the sensor associated with this observation. The term involving measurement errors may be simplified:

$$\delta\Psi\hat{\boldsymbol{X}} = -\delta\boldsymbol{\eta}$$

$$\delta\boldsymbol{\eta}^T = \begin{bmatrix}\hat{\rho}_1\delta\boldsymbol{\lambda}_1^T & \hat{\rho}_2\delta\boldsymbol{\lambda}_2^T & \cdots & \hat{\rho}_N\delta\boldsymbol{\lambda}_N^T\end{bmatrix}$$

Following substitution of this result, the error equations may be expressed in the equivalent form

$$\Psi\delta\hat{\boldsymbol{X}} = \delta\boldsymbol{\eta} + \delta\boldsymbol{Y}$$

It follows that the covariance matrix may be determined by forming the expectation

$$E\{\Psi\delta\hat{\boldsymbol{X}}(\Psi\delta\hat{\boldsymbol{X}})^T\} = \Psi E\{\delta\hat{\boldsymbol{X}}\delta\hat{\boldsymbol{X}}^T\}\Psi^T = E\{\delta\boldsymbol{\eta}\delta\boldsymbol{\eta}^T\} + E\{\delta\boldsymbol{Y}\delta\boldsymbol{Y}^T\}$$

where sensor measurement errors and geolocation errors are uncorrelated ($E\{\delta\boldsymbol{Y}\delta\boldsymbol{\eta}^T\} = 0$). After terms are regrouped, the explicit

solution for the batch covariance matrix is algebraically similar to the least-squares solution for $\hat{\boldsymbol{x}}$:

$$P_B = E\{\delta\hat{\boldsymbol{X}}\delta\hat{\boldsymbol{X}}^T\} = K[E\{\delta\boldsymbol{\eta}\delta\boldsymbol{\eta}^T\} + E\{\delta\boldsymbol{Y}\delta\boldsymbol{Y}^T\}]K^T$$

$$K = (\Psi^T\Psi)^{-1}\Psi^T$$

When successive sets of LOS observations are uncorrelated such that $E\{\delta\boldsymbol{\lambda}_i\delta\boldsymbol{\lambda}_j\} = 0$ for $i \neq j$, the measurement noise matrix $E\{\delta\boldsymbol{\eta}\delta\boldsymbol{\eta}^T\}$ may be expressed in block-diagonal form:

$$E\{\delta\boldsymbol{\eta}\delta\boldsymbol{\eta}^T\}$$

$$= \begin{bmatrix} \hat{\rho}_1^2 E\left\{\delta\boldsymbol{\lambda}_1\delta\boldsymbol{\lambda}_1^T\right\} & O_3 & \cdots & O_3 \\ O_3 & \hat{\rho}_2^2 E\left\{\delta\boldsymbol{\lambda}_2\delta\boldsymbol{\lambda}_2^T\right\} & \cdots & O_3 \\ \vdots & \vdots & \ddots & \vdots \\ O_3 & O_3 & \cdots & \hat{\rho}_N^2 E\left\{\delta\boldsymbol{\lambda}_N\delta\boldsymbol{\lambda}_N^T\right\} \end{bmatrix}$$

Errors $\delta\boldsymbol{\lambda}_n$ in the unit LOS vector arise from measurement errors $\delta\gamma_n$ and $\delta\psi_n$,

$$\delta\boldsymbol{\lambda}_n = \frac{\partial\boldsymbol{\lambda}_n}{\partial\gamma_n}\delta\gamma_n + \frac{\partial\boldsymbol{\lambda}_n}{\partial\psi_n}\delta\psi_n$$

$$\frac{\partial\boldsymbol{\lambda}_n}{\partial\gamma_n} = \Re_n^T \begin{bmatrix} \cos\gamma_n \\ -\sin\gamma_n\sin\psi_n \\ -\sin\gamma_n\cos\psi_n \end{bmatrix}, \qquad \frac{\partial\boldsymbol{\lambda}_n}{\partial\psi_n} = \Re_n^T \begin{bmatrix} 0 \\ \cos\gamma_n\cos\psi_n \\ -\cos\gamma_n\sin\psi_n \end{bmatrix}$$

When errors in elevation and azimuth are uncorrelated ($E\{\delta\gamma_n\delta\psi_n\} = 0$), it follows that

$$E\left\{\delta\boldsymbol{\lambda}_n\delta\boldsymbol{\lambda}_n^T\right\} = \frac{\partial\boldsymbol{\lambda}_n}{\partial\gamma_n}\left(\frac{\partial\boldsymbol{\lambda}_n}{\partial\gamma_n}\right)^T E\left\{\delta\gamma_n^2\right\} + \frac{\partial\boldsymbol{\lambda}_n}{\partial\psi_n}\left(\frac{\partial\boldsymbol{\lambda}_n}{\partial\psi_n}\right)^T E\left\{\delta\psi_n^2\right\}$$

Acknowledgments

The author thanks several individuals for their constructive criticism, comments, and insights concerning this article. These individuals include colleagues at Raytheon (Frederick E. Daum, Michael T. DePlonty, and Jim Huang), the Associate Editor Hari Hablani of The Boeing Company, and three anonymous reviewers.

References

[1]Gorecki, F., and Piehler, M., "Adaptive Estimation of an Accelerating Spacecraft," *Proceedings of the AIAA/AAS Astrodynamics Specialist Conference*, AIAA, Reston, VA, 1986, pp. 283–288.

[2]Fowler, J., "Boost and Post-Boost Target State Estimation with Angles-Only Measurements in a Dynamic Spherical Coordinate System ," *American Astronautical Society*, Paper AAS-91-355, Aug. 1991.

[3]Danis, N., "Space-Based Tactical Ballistic Missile Launch Parameter Estimation," *IEEE Transactions on Aerospace and Electronic Systems*, Vol. 29, No. 2, 1993, pp. 412–424.

[4]Schmidt, G., "Designing Nonlinear Filters Based on Daum's Theory," *Journal of Guidance, Control, and Dynamics*, Vol. 16, No. 2, 1993, pp. 371–376.

[5]Hough, M. E., "Optimal Guidance and Nonlinear Estimation for Interception of Accelerating Targets," *Journal of Guidance, Control, and Dynamics*, Vol. 18, No. 5, 1995, pp. 959–968.

[6]Blackman, S., and Popoli, R., *Design and Analysis of Modern Tracking Systems*, Artech House, Boston, 1999, pp. 293–303.

[7]Li, Y., Kirubarajan, T., Bar-Shalom, Y., and Yeddanapudi, M., "Trajectory and Launch Point Estimation for Ballistic Missiles from Boost Phase LOS Measurements," *Proceedings of the IEEE 1999 Aerospace Conference*, Vol. 4, IEEE Publications, Piscataway, NJ, 1999, pp. 425–442.

[8]Blackman, S., and Popoli, R., *Design and Analysis of Modern Tracking Systems*, Artech House, Boston, 1999, pp. 241–250.

[9]Crosson, E., Romine, J., Willner, D., and Kusiak, S., "Boost-Phase Acceleration Estimation," *Proceedings of the IEEE 2000 International Radar Conference*, IEEE Publications, Piscataway, NJ, 2000, pp. 210–214.

[10]Hough, M. E., "Nonlinear Recursive Filter for Boost Trajectories," *Journal of Guidance, Control, and Dynamics*, Vol. 24, No. 5, 2001, pp. 991–997.

[11]Van Zandt, J., "Boost Phase Tracking with an Unscented Filter," *Proceedings of SPIE, International Society for Optical Engineering*, edited by O. Drummond, Society of Photo-Optical Instrumentation Engineers, Vol. 4728, Bellingham, WA, 2002, pp. 263–274.

[12]Battin, R., *An Introduction to the Mathematics and Methods of Astrodynamics*, AIAA Education Series, AIAA, New York, 1987, pp. 138–139.

[13]Gelb, A. (ed.), *Applied Optimal Estimation*, MIT Press, Cambridge, MA, 1974, pp. 190, 191.

[14]Bell, B., and Cathey, F., "The Iterated Kalman Filter Update as a Gauss–Newton Method," *IEEE Transactions on Automatic Control*, Vol. 38, No. 2, 1993, pp. 294–297.

[15]Magill, D., "Optimal Adaptive Estimation of Sampled Stochastic Processes," *IEEE Transactions on Automatic Control*, Vol. AC-10, No. 4, 1965, pp. 434–439.

[16]Blom, H., and Bar-Shalom, Y., "The Interacting Multiple Model Algorithm for Systems with Markovian Switching Coefficients," *IEEE Transactions on Automatic Control*, Vol. 33, No. 8, 1988, pp. 780–783.

[17]Averbuch, A., Itzikowitz, S., and Kapon, T., "Radar Target Tracking—Viterbi versus IMM," *IEEE Transactions on Aerospace and Electronic Systems*, Vol. AES-27, No. 3, 1991, pp. 550–563.

[18]Mazor, E., Averbuch, A., Bar-Shalom, Y., and Dayan, J., "Interacting Multiple Model Methods in Target Tracking: A Survey," *IEEE Transactions on Aerospace and Electronic Systems*, Vol. 34, No. 1, 1998, pp. 103–123.

[19]Blackman, S. and Popoli, R., *Design and Analysis of Modern Tracking Systems*, Artech House, Boston, 1999, pp. 221–241.

[20]Hough, M. E., "Improved Performance of Recursive Tracking Filters Using Batch Initialization and Process Noise Adaptation," *Journal of Guidance, Control, and Dynamics*, Vol. 22, No. 5, 1999, pp. 675–681.